PAPER Special Section on Ultra Wideband Systems

On Rake Reception of Ultra Wideband Signals over Multipath Channels from Energy Capture Perspective

Mohammad Azizur RAHMAN[†a)], ***Student Member***, **Shigenobu SASAKI**[†], **Jie ZHOU**[†*], ***and*** **Hisakazu KIKUCHI**[†], ***Members***

SUMMARY Performance of Rake reception of Ultra Wideband (UWB) signals is evaluated from energy capture perspective. In addition to ordinary all Rake (ARake) and selective Rake (SRake) receivers which are considered in conventional spread spectrum communications, we introduce optimum ARake and SRake receivers which include the estimation of delay of the combining multipaths. Impact of pulse-width is discussed on their performances considering the relationship between pulse-width and fading. Time hopping M-ary pulse position modulation (TH-MPPM) and binary phase shift keying (TH-BPSK) are considered as modulation schemes. Extensive simulation results are presented showing the performances of the Rakes introduced using IEEE 802.15.3a UWB channel models (CM1 to CM3). Performance of MPPM is shown for various values of M and modulation parameters. The impact of pulse-width is illustrated mainly using BPSK. It is shown that the total energy capture (i.e. by ARake) strongly depends on the pulse-width, and the shorter the pulse-width the more is the amount. The energy capture also varies a lot for employing either optimum or ordinary Raking method. Energy capture by SRake additionally strongly depends on the number of combined paths until the number is ≤ 20 for optimum SRake and ≤ 10 for ordinary SRake; however, afterwards saturating effects are seen. Several aspects regarding the performance versus complexity issue of Rake receivers are also discussed.

key words: *ultra wideband, multipath, Rake reception, energy capture, pulse-width*

1. Introduction

Ultra Wideband (UWB) technology has been one of the most promising new technologies for wireless communications [1]. Although there are several alternatives to design UWB systems, in this work we are interested in time hopping (TH) impulse radio (IR) UWB communications [2]. One of the most attractive features of the UWB signals is identified as their better multipath resolvability [3]. It is known that Rake receivers that are often employed in conventional spread spectrum communications are attractive solutions in UWB communications over multipath channels as well [4], [5]. Throughout this paper we use correlation type Rake receivers [4] that use a reference signal consisting of pulses matched with an isolated received pulse.

An *all Rake* (*ARake*) is one that collects all possible resolved multipaths and combines the energy by maximal ratio combining (MRC) [6], [7]. However, there exist hundreds of resolved multipaths for UWB systems. Also, the number of resolvable paths increases with communication distance and bandwidth [3]. As a consequence, ARake reception will cost unacceptable complexity though the performance improvement is expected. As a compromise between performance and complexity, the concept of *selective Rake* (*SRake*) receiver has evolved in literature [3], [6], [7]. SRake combines L_c paths which has the first to the L_cth largest magnitude out of all resolved paths $L(L_c < L)$ by MRC.

In conventional Rake type receivers, each correlator is placed at each integer multiple of the pulse-width. ARake and SRake receivers that follow this method, we call them *ordinary all Rake* (*Or_ARake*) and *ordinary selective Rake* (*Or_SRake*) receiver respectively. In UWB communications, pulse waveform is not radiated continuously, but at some time during the pulse repetition interval. Additionally, multipaths are not usually received at delays that are multiples of pulse-width. It offers another option for Rake reception of UWB signals by estimating the delays of the multipaths. System performance depends on the fraction of energy that can be captured by the Rake receiver [5]. If the estimation of optimal delays of the multipaths is available in spite of increasing complexity, it is suggested that more energy could be captured by Rake receiver [3], [5]. ARake and SRake receivers that estimate the best delays and place the correlators at those delays, we call them *optimum all Rake* (*Op_ARake*) and *optimum selective Rake* (*Op_SRake*) receiver respectively. Although the concept of optimum ARake and SRake would be an attractive solution to fight multipath fading, no performance comparison with ordinary Rake has been carried out yet either for ARake or SRake.

Because the UWB channel is very frequency selective, the channel response should be highly dependent on the width of the pulse transmitted. The amount of fading experienced by the signal should depend on the pulse-width and so as the performances of the Rake receivers. However, many of previous works on Rake reception of UWB signals were mainly based on specific pulse-width [3], [5], [8]–[16]. Additionally, there have been no previous papers considering both ordinary and optimum Rakes discussing the performance versus complexity trade-off in realistic UWB channels.

In this paper, we discuss the effects of employing or-

Manuscript received August 23, 2004.
Manuscript revised December 3, 2004.
Final manuscript received May 18, 2005.

[†]The authors are with the Department of Electrical and Electronic Engineering, Niigata University, Niigata-shi, 950-2181 Japan.
[*]Presently, with the Department of Information and Communications, Nanjing University of Information Science and Technology, China.
a) E-mail: aziz@telecom0.eng.niigata-u.ac.jp

DOI: 10.1093/ietfec/e88–a.9.2339

dinary and optimum methods of Raking, pulse-width variations and various modulation schemes on the performance of the above-mentioned Rake receivers over realistic UWB channel models to answer many previously unanswered questions described above [17]. We consider time hopping M-ary PPM (TH-MPPM) including both overlapped and orthogonal signal set for MPPM [8] and TH-binary phase shift keying (TH-BPSK). First, we present a general framework on calculating error probabilities for the above-mentioned signaling schemes over multipath channels. Then, we discuss the effect of pulse-width on fading from the view point of indoor channel statistics. Finally, we present extensive simulation results using IEEE 802.15.3a UWB channel models (CM1 to CM3) [18] investigating the effects of fading due to non line of sight (NLOS) reception and increase in communication distance. We present error performances of the Rakes introduced and discuss several aspects of performance versus complexity issue of Rake receiver considering several points including the effect of pulse-width from energy capture perspective.

Our paper is organized as follows. In the next section we describe the signaling scheme, the receivers considered and derive the error probabilities. In Sect. 3, we discuss the relationship between pulse-width and fading experienced over indoor multipath channels. In Sect. 4, we first present simulation model and then simulation results with relevant discussions. Finally, we conclude in Sect. 5.

2. System Model

2.1 Signals and Channel Model

We consider a TH system, a block diagram of which is shown in Fig. 1. A transmitted symbol of the k-th user in TH-MPPM system is represented by [2],

$$s_d^{(k)}(t) = \beta_d \sqrt{E_p} \sum_{j=0}^{N_s-1} w(t - jT_f - C_j^{(k)} T_c - \delta_d^{(k)}), \quad 0 \le t \le N_s T_f \tag{1}$$

where $\delta_d \in \{\delta_0 = 0 < \delta_1 < \delta_2 \ldots < \delta_{M-1}\}$ represent the time shifts that identify the symbol, d represents data that can be any one from a total of M symbols, $d \in \{0, 1, 2, \cdots, M-1\}, \beta_d = 1$ for all d, T_f is the frame time, T_c is the chip time, $C_j^{(k)}$ is the user dependent TH code, N_s is the total number of frames used to represent one symbol, E_p is the transmitted energy of each pulse and $w(t)$ is the unit energy pulse used for UWB communication. Let us assume that the pulse-width is T_p and the system bandwidth is $W \approx 1/T_p$.

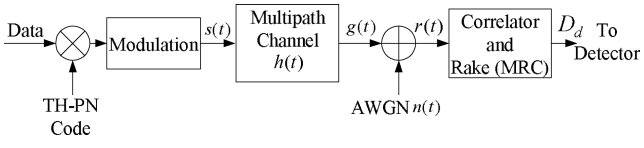

Fig. 1 Block diagram of the system.

It is assumed that each frame is subdivided into N_c equally spaced chips giving, $T_f = N_c T_c$, and symbol duration $T_s = N_s T_f$. It is further assumed that $\delta_{M-1} + T_p \le T_c$. The user dependent TH code $C_j^{(k)}$ is a random number uniform over $\{0, 1, \ldots, N_c - 1\}$ and has a periodicity equal to N_s. The signaling structure of TH-MPPM for an arbitrary user k is shown in Fig. 2.

For the MPPM under consideration, it will be called orthogonal MPPM while $\delta_{i+1} - \delta_i = T_p$ and overlapped MPPM, generally speaking, while $\delta_{i+1} - \delta_i < T_p$, $i = 0, 1, \cdots, M-2$. We consider the well known received monocycle pulse shape as shown in Fig. 3. This provides a minimum autocorrelation of -0.6183 at delays $0.212T_p$. If $\delta_{i+1} - \delta_i = 0.212T_p$, $i = 0, 1, \cdots, M-2$ is placed, it maximizes the Euclidian distance among the MPPM signal sets. It is called the optimum overlapped MPPM [8].

We consider a single user environment. Hence, leaving the superscript k from now on, the received signal can be given by [9],

$$r_d(t) = s_d(t) * h(t) + n(t)$$

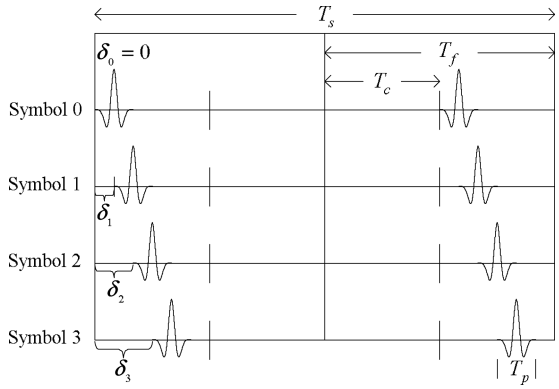

Fig. 2 TH-MPPM signals for an arbitrary user k with $M = 4, N_s = 2, N_c = 2$ and TH sequence $C^{(k)} = \{0, 1\}$.

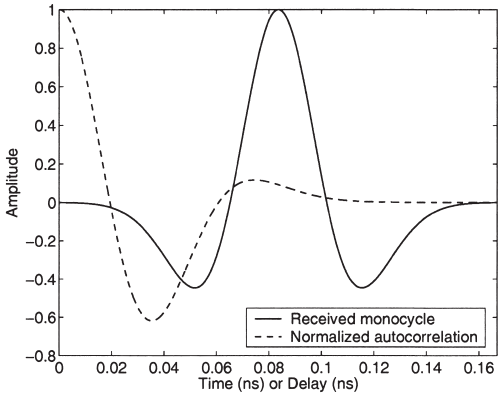

Fig. 3 Received monocycle pulse given by $[1 - 4\pi\{(t - T_p/2)/\tau_m\}^2] \exp[(-2\pi)\{(t - T_p/2)/\tau_m\}^2]$ and its normalized autocorrelation for $T_p = 0.167$ ns and $\tau_m = 0.39T_p$. The minimum correlation of -0.6183 occurs at delay $= 0.212T_p$ ns.

$$= \sqrt{E_p}\sum_{j=0}^{N_s-1} g(t - jT_f - C_jT_c - \delta_d) + n(t) \qquad (2)$$

where $h(t)$ is the channel impulse response, $n(t)$ is additive white Gaussian noise (AWGN) and $*$ represents convolution. Note that though the transmitted pulse $w(t)$ had unit energy, multipath profile of the pulse $g(t) = w(t) * h(t)$ has energy $E_g = \int_0^{T_g} g^2(t)dt, \leq 1$, because of path loss. Here T_g is the duration of the multipath profile $g(t)$ known as the maximum delay spread of the channel.

2.2 Receiver Model

At the end of the multipath channel Rake type receiver is used. The Rake receiver is implemented by using delayed versions of the reference signal $\hat{v}_d(t)$ [4]. The output of the correlator corresponding to the l-th finger of the Rake receiver can be given by

$$Z_{d,l} = \int_{-\infty}^{+\infty} r_d(t)\hat{v}_d(t - \tau_l)dt, \qquad (3)$$
$$l = 0, 1, \cdots, L_o - 1 \text{ for each } d = 0, 1, \cdots, M - 1$$

Note that we need to use M correlators [19]. Here L_o is the number of paths captured and τ_l is the delay where the l-th correlator is placed. For an Or_ARake, $L_o = L_{or}$ where L_{or} is the total number of resolved paths by the Or_ARake and $L_{or} = \lceil T_g/T_p \rceil$, $\lceil . \rceil$ being ceiling function. And $\tau_l = \tau_{or} = lT_p, l = 0, 1, 2, \cdots, L_{or} - 1$. For an Or_SRake, $L_o = L_c$ where L_c is the number of combined paths and τ_l are locations of the best L_c paths from τ_{or}. For an Op_ARake, $L_o = L_{op}$ where L_{op} is the total number of resolved paths by the Op_ARake. In this case, locations of the paths $\tau_l = \tau_{op}, l = 0, 1, 2, \cdots, L_{op} - 1$ depend entirely on the channel. In other words, Op_ARake places all its L_{op} paths so as to maximize the captured energy. Op_SRake captures $L_o = L_c$ best paths choosing best L_c locations from τ_{op}. Figure 4 shows a simplified representation of the finger (correlator) placement of Or_ARake and Op_ARake. Note that in ordinary method, finger placements are simply T_p apart. In optimum method, fingers are first placed in the peaks of the multipath intensity profile (MIP). Later, the rest of the MIP is covered in such a way that fingers can be placed slightly closer than T_p to maximize the captured energy, as long as the correlation is nearly zero (see Fig. 3).

We assume that the following normalized reference signals are employed

$$\hat{v}_d(t) = \sum_{j=0}^{N_s-1} \frac{1}{\sqrt{N_s}} w_{rec}(t - jT_f - C_jT_c - \delta_d),$$
$$0 \leq t \leq N_sT_f \text{ and } d = 0, 1, \cdots, M - 1 \qquad (4)$$

where $w_{rec}(t)$ is a unit energy pulse that matches well with an isolated received pulse. Without loss of generality, let us consider that 'symbol 0' is transmitted. The received signal, neglecting the transmission delay, can be given by

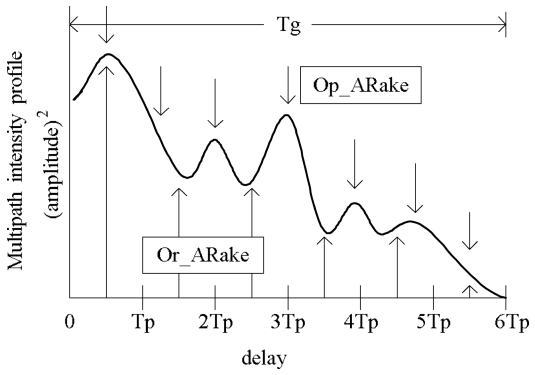

Fig. 4 Placing the correlators for Or_ARake and Op_ARake in an arbitrary multipath intensity profile. Bottom and top arrows denote the positions of the center of the template for Or_ARake and Op_ARake respectively.

$$r_0(t) = \sqrt{E_p}\sum_{j=0}^{N_s-1} g(t - jT_f - C_jT_c) + n(t) \qquad (5)$$

Let us define a cross-correlation function between $g(t)$ and $w_{rec}(t)$ at delay τ to be [9],

$$\alpha(\tau) = \int_{-\infty}^{+\infty} g(t)w_{rec}(t - \tau)dt \qquad (6)$$

Note that $\alpha(\tau) = 0$ if $\tau \leq -T_p$ or $\tau \geq T_g$. As a result (3) can be rewritten as,

$$Z_{d,l} = \sqrt{\zeta}\alpha(\tau_l + \delta_d) + n_{d,l} \qquad (7)$$
$$l = 0, 1, \cdots, L_o - 1 \text{ for each } d = 0, 1, \cdots, M - 1$$

where $n_{d,l} = \int_{-\infty}^{+\infty} n(t)\hat{v}_d(t - \tau_l)dt$, $l = 0, 1, \cdots, L_o - 1$ for each $d = 0, 1, \cdots, M - 1$ and $\zeta = N_sE_pE_g$.

A maximal ratio combiner (MRC) is used to combine the multipath signals. It is assumed that the MRC can correctly predict the channel parameters: amplitude, phase and delay as needed. So, MRC output per decision hypotheses becomes

$$Z_d = \sqrt{\zeta}\sum_{l=0}^{L_o-1} \alpha(\tau_l)Z_{d,l},\ d = 0, 1, \cdots, M - 1$$
$$= \zeta\sum_{l=0}^{L_o-1} \alpha(\tau_l)\alpha(\tau_l + \delta_d) + n_d \qquad (8)$$

where $n_d = \sqrt{\zeta}\sum_{l=0}^{L_o-1} \alpha(\tau_l)n_{d,l},\ d = 0, 1, \cdots, M - 1$.

2.3 Error Probabilities

Now, from (8) the decision variable can be written as,

$$D_0 = Z_0 - \sum_{d=1}^{M-1} Z_d \qquad (9)$$

Here, D_0 is assumed to be conditionally Gaussian (conditioned on the channel parameters) with mean [4]

$$E[D_0] = \zeta \sum_{l=0}^{L_o-1} \mathcal{E}_l^{(0)} \tag{10}$$

and variance [4], $\mathrm{var}[D_0] = E[D_0^2] - E[D_0]^2$ which can be rewritten as

$$\mathrm{var}[D_0] = \zeta N_o \sum_{l=0}^{L_o-1} \mathcal{E}_l^{(0)} \tag{11}$$

where N_o is the one sided AWGN variance and

$$\mathcal{E}_l^{(0)} = \alpha^2(\tau_l) - \sum_{i=1}^{M-1} \alpha(\tau_l)\alpha(\tau_l + \delta_i) \tag{12}$$

The conditional probability of symbol error (again conditioned on the channel parameters and the 'symbol 0' is sent) can be given by

$$\begin{aligned} SEP_d &= P[D_d < 0, \text{ symbol } d \text{ sent}] \\ &= Q\left(\sqrt{\frac{E[D_d]^2}{\mathrm{var}[D_d]}}\right) = Q\left(\sqrt{\frac{\zeta \sum_{l=0}^{L_o-1} \mathcal{E}_l^{(d)}}{N_o}}\right) \end{aligned} \tag{13}$$

with $d = 0$ where $Q(x) = (2\pi)^{-1/2} \int_x^\infty exp(-u^2/2)du$. If 'symbol d' is transmitted where $d = 1, 2, \cdots, M-2$, similarly, it can be shown that the symbol error probability (SEP) is given by (13) with

$$\begin{aligned} \mathcal{E}_l^{(d)} &= \alpha^2(\tau_l) - \sum_{i=0}^{d-1} \alpha(\tau_l)\alpha(\tau_l - (\delta_d - \delta_i)) \\ &\quad - \sum_{i=d+1}^{M-1} \alpha(\tau_l)\alpha(\tau_l + (\delta_i - \delta_d)) \end{aligned} \tag{14}$$

And for 'symbol $M-1$,' the SEP is given by (13) with

$$\mathcal{E}_l^{(d)} = \alpha^2(\tau_l) - \sum_{i=0}^{M-2} \alpha(\tau_l)\alpha(\tau_l - (\delta_{M-1} - \delta_i)) \tag{15}$$

where $d = M-1$. Finally, the average SEP for TH-MPPM is

$$\overline{SEP} = \frac{1}{M} \sum_{d=0}^{M-1} SEP_d \tag{16}$$

Equations (13) and (16) representing SEP for TH-MPPM that uses (12), (14), (15) shown above can be easily simplified for an AWGN channel as a function of the normalized correlation function of an isolated received pulse $\gamma(\delta)$ which is given by, $\gamma(\delta) = \int_{-\infty}^{+\infty} w_{rec}(t) w_{rec}(t-\delta), > -1$.

By assuming $M = 2$ and $\delta_d \in \{(\delta_0 = 0) < (\delta_1 = \delta)\}$ in the above analysis, the bit error probability (BEP) equations for TH-BPPM can be obtained [20]. For TH-BPSK system because pulses of opposite signs are used to represent bits '0' and '1,' we get $\beta_0 = -\beta_1$ and $\delta_0 = \delta_1 = 0$ in (1). Following similar procedure as given above, we get equal bit error rate for both '0' and '1' in BPSK given by

$$BEP_{BPSK} = Q\left(\sqrt{\frac{2\zeta \sum_{l=0}^{L_o-1} \alpha^2(\tau_l)}{N_o}}\right) \tag{17}$$

3. Pulse-Width vs. Fading

In this section we discuss the effects of pulse-width on the received channel response and its impact on Rake reception. It is well accepted that increasing spreading bandwidth increases multipath resolvability [5]–[7]. The energy in the received multipath profile is received generally through two types of receptions. These are isolated receptions and overlapped receptions (i.e. diffused paths). If a single ray (path) is received during one pulse duration, we call it an isolated path. Isolated paths experience no fading. Else, if more than one ray is received within one pulse duration, we call those overlapped paths. Overlapped paths are responsible for the multipath fading (amplitude fluctuations).

If an impulse is transmitted over a multipath channel, the received multipath profile is the impulse response of the channel where all the receptions are received as isolated paths. At reasonably high SNR, most of the energy present in the channel can be captured by Rake if delay estimation strategy is employed. An impulse can be considered to have a pulse-width that tends to zero. But as practical communications use wider pulses, some paths will be received as overlapped receptions. So, multipath fading will exist the amount of which will depend on the pulse-width. It can be understood intuitively that multipath resolvability and hence the fraction of energy that can be captured depends on how the total number of received multipaths and their energy content is divided into isolated and overlapped receptions. This, in turn, depends on pulse-width other than the channel.

Recently double Poisson process of [21] has been proposed with some modifications for the arrivals of multipath components in indoor UWB communications [18]. Two Poisson processes have been defined: one for the arrival of (the first component of) clusters with average cluster arrival rate Λ and another for the arrival of rays within the clusters with average ray arrival rate λ [18], [21]. To explore the impact of pulse-width variations on the received profile, we assume that rays of any of the previous clusters have no effect on the current cluster (a reasonable assumption, especially in exponentially decaying power delay profile [18], [21], [22]). Upon this assumption, the approximate probability that we will have at least one reception within an arbitrary short duration of time Δt is $(\Lambda + \lambda)\Delta t$ [23]. The probability that there will be no reception within Δt is simply $1 - (\Lambda + \lambda)\Delta t$. For a pulse duration of T_p, we assume that there exist S time slots of duration Δt where $S = T_p/\Delta t$ (T_p is assumed to be divisible by Δt). So, after reception of a path at any time, the probability that there will be no new reception for next T_p duration is $\{1 - (\Lambda + \lambda)\Delta t\}^S$. Also, the probability that there was no reception for T_p duration before receiving that path is the same $\{1 - (\Lambda + \lambda)\Delta t\}^S$. So the probability of an isolated reception becomes equal to $\{1 - (\Lambda + \lambda)\Delta t\}^{2S}$. An illustration of it is shown in Fig. 5 using $\Lambda = 1/43, \lambda = 2.5, \Delta t = 0.01$ ns corresponding to IEEE 802.15.3a CM1 of [18] for $0 < T_p \leq 2$ ns.

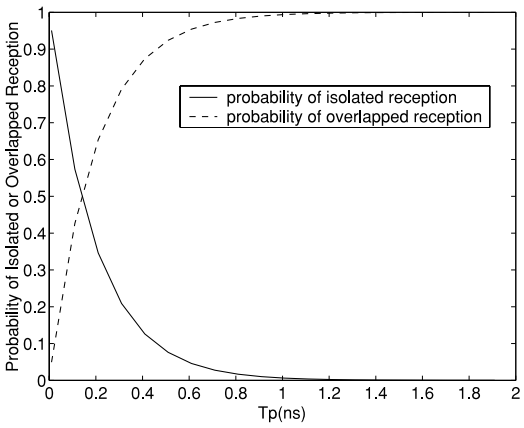

Fig. 5 Probabilities of isolated and overlapped receptions vs. pulse-width for $\Lambda = 1/43$, $\lambda = 2.5$, $\Delta t = 0.01$ ns corresponding to IEEE 802.15.3a CM1.

4. Computer Simulations

4.1 Simulation Model

In this section, the ideas developed in the previous sections are illustrated by providing extensive simulation examples. We use IEEE 802.15.3a UWB indoor multipath channel models (Table 1) for simulations [18], [24]. As we have mentioned earlier, IEEE 802.15.3a models use the modified Saleh-Valenzuela indoor channel model [21]. The programs provided in [18] are used to produce the discrete time impulse response with continuous time arrival and amplitude values. The impulse response of the i-th realization can be given by [18],

$$h_i(t) = X_i \sum_{l=0}^{N_{cl}} \sum_{j=0}^{N_{ray}} a^i_{j,l} \delta_D(t - T^i_l - \tau^i_{j,l}) \tag{18}$$

where δ_D is Dirac delta function, $\{a^i_{j,l}\}$ are the multipath gain coefficients, $\{T^i_l\}$ is the delay of the l-th cluster, $\{\tau^i_{j,l}\}$ is the delay of the j-th multipath component (ray) relative to the l-th cluster arrival time $\{T^i_l\}$, $\{X_i\}$ is the log-normal shadowing term, N_{cl} is the total number of clusters and N_{ray} is the number of rays in each cluster.

The main simulation parameters for the simulation process are shown in Table 2. The received monocycle pulse shape [5],

$$w_{rec}(t) = \left[1 - 4\pi\left(\frac{t - T_p/2}{\tau_m}\right)^2\right] \times \exp\left[(-2\pi)\left(\frac{t - T_p/2}{\tau_m}\right)^2\right] \tag{19}$$

as shown in Fig. 3 is used where T_p is the pulse-width and $\tau_m = 0.39T_p$. As mentioned in Sect. 2, this provides a minimum correlation of -0.6183 at delay $\tau_{op} = 0.212T_p$. As a result, for optimum overlapped MPPM we set, $\delta_i = i\tau_{op}$ and for orthogonal MPPM, we set $\delta_i = iT_p$, with $\beta_i = 1$ for both, $i = 0, 1, 2, \cdots, M-1$. For BPSK, $\delta_0 = \delta_1 = 0$ and $\beta_0 = -\beta_1$.

Table 1 Channel models.

Model	LOS/NLOS	Distance
CM1	LOS	0–4 m
CM2	NLOS	0–4 m
CM3	NLOS	4–10 m

Table 2 Simulation parameters for each channel model.

N_s	1
N_c	1
Data Rate	3 Mega symbols/s
Modulation	BPSK and MPPM
ISI and ICI	No
Receivers	*Op_ARake, Or_ARake, Op_SRake* and *Or_SRake,* MRC
T_p	0.167 ns to 4.0 ns
Pulse Shape	Received monocycle

Rake performance is evaluated from energy capture perspective [3], [5]. Simply $N_s = N_c = 1$ and $T_s = T_f = T_c = 333$ ns are used. This helps us assume the multipath components to be uncorrelated even for closely spaced Rake fingers [6], [7]. Our system is assumed to be free from inter-chip-interference (ICI) and inter-symbol-interference (ISI). In addition, ideal channel estimations are assumed available. Amplitude and phase of each multipath component are assumed known for Or_ARake; and amplitude, phase and delay of each multipath component are assumed known for Op_ARake. Furthermore, for an SRake with L_c paths, locations of L_c best paths are assumed known for respective ordinary or optimum method. Received energies are normalized over E_g to be able to make a fair comparison over the channel models.

4.2 Simulation Results and Discussions

4.2.1 Performance of ARake

A. Performance vs. Pulse-Width

Figure 6 shows two truncated noise-less channel responses over CM1 for transmitting unit energy pulses of duration 0.167 ns and 1.0 ns. It can be seen that the use of shorter pulse provides more isolated receptions and less amplitude fluctuations (fading). Figure 7 shows the BEP performance of both types of ARake over CM1 for BPSK. For certain pulse-width, Op_ARake is found to perform better than Or_ARake. At BEP = 10^{-5}, use of Op_ARake experiences an SNR loss of -0.6 dB for using $T_p = 0.167$ ns whereas -4.35 dB for using $T_p = 2.0$ ns as compared to performance in AWGN. The similar SNR losses for using Or_ARake are -6.5 dB and -8.5 dB respectively. However, at any specific SNR, the BEP advantage due to the pulse-width shortening decreases at low SNR. This is because, a number of low-energy-paths get submerged below noise level whose energies can't be captured.

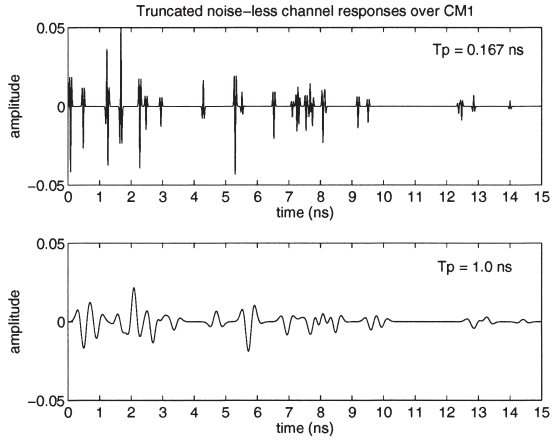

Fig. 6 Truncated noise-less channel responses over CM1 for transmitting unit energy pulses of duration 0.167 ns (top) and 1.0 ns (bottom).

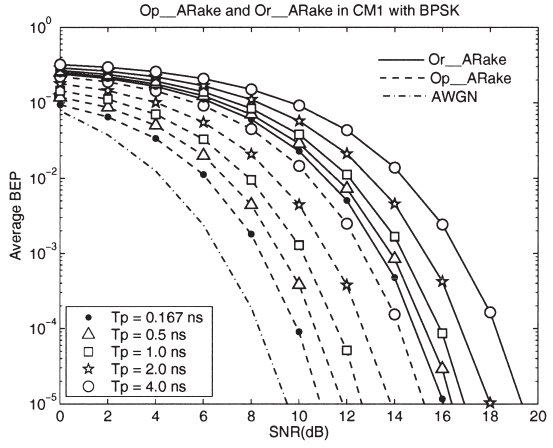

Fig. 7 BEP for ARake in CM1 with BPSK.

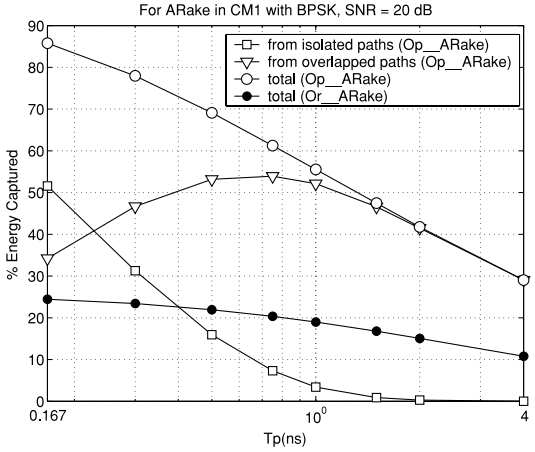

Fig. 8 Percentage energy capture by ARake in CM1 with BPSK. SNR = 20 dB.

B. Energy Capture vs. Pulse-Width

Figure 8 shows the percentage energy capture by ARake vs. pulse-width for CM1. BPSK is used as modulation and

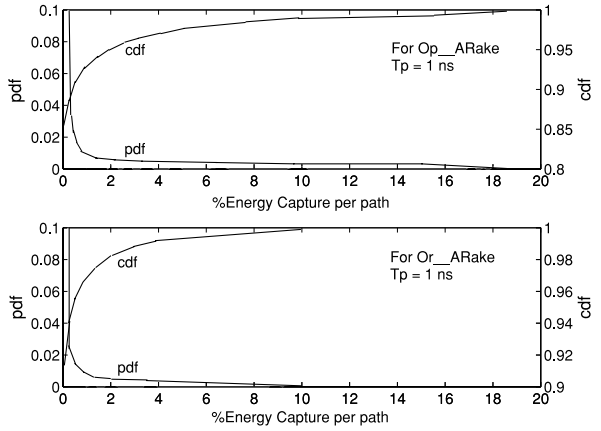

Fig. 9 Statistics of the percentage energy capture per path for Op_ARake and Or_ARake (CM1, BPSK, T_p = 1 ns). Here pdf (left y-axes) stands for probability density function, and cdf (right y-axes) stands for cumulative distribution function = Probability {percentage energy capture per path ≤ abscissa}.

SNR is set at 20 dB. An Op_ARake can identify the locations of the isolated paths and if a reasonably high SNR is maintained, the energy can be captured almost entirely irrespective of the pulse-width. In harmony with the probabilistic prediction presented in the previous section, the net contribution in the total energy capture from the isolated paths increases exponentially while the pulse-width is shortened. Percentage energy coming from the overlapped paths first increases with pulse-width shortening and then starts decreasing. This is because the amount of energy received through overlapped paths decreases considerably while the pulse-width is shortened. The total energy captured by an Op_ARake is the summation of energies from both the isolated and overlapped paths that increases monotonically while we shorten the pulse-width. However, finally slightly diminishing returns are noticed. Note that the total energy present in the multipath profile doesn't change that much with pulse-width variations [25]. But, the amount of energy that can be captured varies considerably due to variations in the amount of fading experienced.

On the other hand, an Or_ARake tries to capture energy blindly by placing the correlator at each multiple of the pulse-width. Since it cannot distinguish between isolated and overlapped receptions, most of the received paths experience partial correlation and captured energy decreases considerably as compared with Op_ARake. Energy capture increases with pulse-width shortening for both Op_ARake and Or_ARake, but in Or_ARake it increases with much slower rate. Additionally, Or_ARake output experiences greater diminishing effects much earlier. However, the performance difference between Op_ARake and Or_ARake decreases as the pulse-width becomes wider.

Figure 9 shows the the probability density function (pdf) and cumulative distribution function (cdf) of the percentage energy capture per path for both types of the ARakes in CM1 with T_p = 1 ns considering a noise-less case. It is seen from pdf that the probability of receiving

paths containing infinitesimally small energy is very high, whearas the probability of receiving high energy paths decreases. Also both from pdf and cdf, the maximum energy content of a path is much lower in Or_ARake. Here note that in a multipath profile, the paths (i.e. the correlator placements) are different for ordinary and optimum methods. Furthermore, the energy content per path and the energy that can be captured from that path are different due to fading.

C. Performance with MPPM

In Figs. 10 and 11 we present average SEP vs. symbol SNR performance of Op_ARake and Or_ARake in CM1 for optimum overlapped and orthogonal MPPM respectively with $M = 2$, 4 and 8. Symbol energy is kept constant irrespective of the value of M. For optimum overlapped MPPM (Fig. 10), it is found at low SNR that the performance becomes slightly better as M is increased. However, multiple crossovers are seen afterwards as SNR is increased. Curves for wider pulse-widths are seen to experience crossovers at higher SEP and SNR sets. Note that these crossovers appear only in optimum overlapped MPPM, not in orthogonal MPPM. In optimum overlapped MPPM, the delay between adjacent pulses $\delta_{i+1} - \delta_i, i = 0, 1, \cdots, M-2$ is placed where the adjacent pulse has the largest Euclidian distance. In this case, pulses next to the adjacent pulse could have positive crosscorrelation according to Fig. 3. It affects the SEP curves in Fig. 10 and crossovers occur among the curves for different M at midium to high SNR. Additionally, the curves for multipath take similar looking shapes as those for AWGN because the autocorrelation property of a multipath profile doesn't deviate that much from that of a single pulse [3], [16].

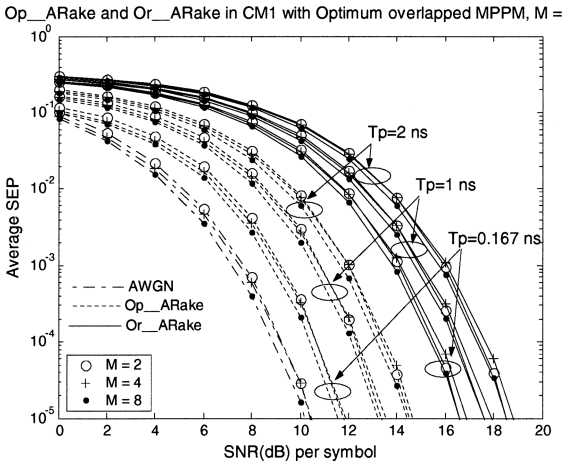

Fig. 10 SEP of optimum overlapped MPPM with all $\delta_i = 0.212iT_p, i = 0, 1, \cdots M-1$ over CM1 while ARakes are employed.

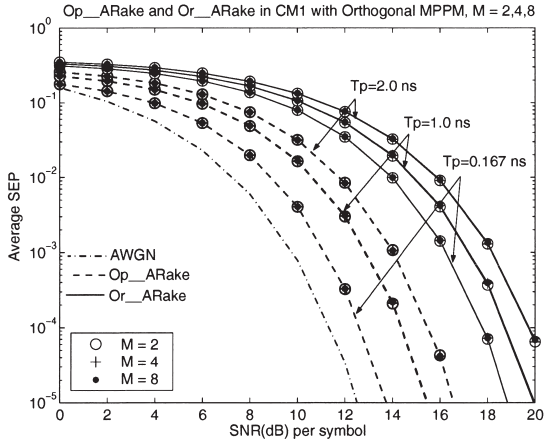

Fig. 11 SEP of orthogonal MPPM with $\delta_i = iT_p, i = 0, 1, 2, \cdots, M-1$ over CM1 while ARakes are employed.

For orthogonal MPPM (Fig. 11), extensive simulations have shown that if $\delta_{i+1} - \delta_i, i = 0, 1, \cdots, M-2$ are set larger than or equal to the minimum delay beyond which pulse autocorrelation is zero or negligible (see Fig. 3), system performance remains almost unchanged. Performance also remains nearly unchanged with variations in the value of M, though (12)–(15) predicts performance variations with M even when the symbol SNR is fixed. This is again because the multipath profiles are not that much correlated and the orthogonality of the transmitted pulses are more or less reserved [3], [16].

Performance degradation for using MPPM as compared to BPSK doesn't depend on pulse-width. The cost incurred in SNR for using optimum overlapped MPPM (Fig. 10) rather than using BPSK (Fig. 7) is less than around -1 dB at SEP = 10^{-5}. The similar cost for using orthogonal MPPM (Fig. 11) is around -2.85 dB.

D. Performance in Different Channel Models

Performance in CM2 as compared with CM1 would help us understand the effects of LOS/NLOS receptions on Rake reception over the same communication distance whereas performance in CM3 would help us understand the effects of fading due to distance. Note that [18] doesn't include path loss model and hence neither do we. Performances over different CMs are compared under same SNR.

Figure 12 shows BEP performance comparisons over CM1, 2 and 3 while Op_ARake and Or_ARake are used. BPSK is considered. Op_ARake is found to be more sensitive to fading due to the distance of communication rather than LOS/NLOS receptions over the same distance. Hence, Op_ARake performs comparably over CM1 and CM2. However, performance over CM3 as compared with CM1 experiences an SNR loss of -0.3 dB for $T_p = 0.167$ns and -1.0 dB for $T_p = 2$ ns at BEP of 10^{-5}. Or_ARake is found to be sensitive to fading due to both NLOS receptions and communication distance. In a LOS channel (such as CM1), there exists a comparatively strong first path (see Fig. 6) that is always captured by an Or_ARake. As a result, Or_ARake performance over CM2 as compared with CM1 experiences an SNR loss of -1.0 dB at BEP= 10^{-5} which seems not to depend on T_p. Performance over CM3 experiences a loss of -1.2 dB for $T_p = 0.167$ns and -2.2 dB for $T_p = 2$ ns.

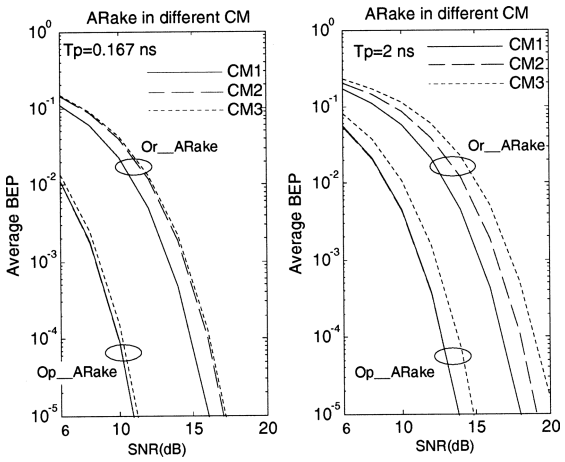

Fig. 12 BEP for Op_ARake and Or_ARake over CM1, 2 and 3 for T_p = 0.167 ns and 2.0 ns while BPSK is used as modulation.

Table 3 Number of paths captured by ARake. (SNR = 20 dB, BPSK) (Notation: $\overline{X}$ represents mean value of X)

T_p(ns)	CM1 $\overline{T_g}$ = 78.87 ns		CM2 $\overline{T_g}$ = 118 ns		CM3 $\overline{T_g}$ = 203.6 ns	
	$\overline{L_{or}}$	$\overline{L_{op}}$	$\overline{L_{or}}$	$\overline{L_{op}}$	$\overline{L_{or}}$	$\overline{L_{op}}$
0.167	473	540	707	787	1220	1364
0.5	158	175	236	257	408	443
1.0	79	87	118	129	204	220
2.0	40	45	59	66	102	111

4.2.2 Performance of SRake

A. Energy Capture vs. L_c in Different Channel Models

Table 3 shows some of the simulation results namely mean maximum delay spread and mean number of combined paths by ARake for CM1, CM2 and CM3. The mean number of combined paths helps us realize the implementation complexity that renders ARake impractical. Figure 13 shows percentage energy capture by Or_SRake and Op_SRake versus selective combined paths L_c in all three channel models. It's worth noting that the initial rate of increment of the energy capture with L_c is the fastest in CM1 and the slowest in CM3 leaving CM2 in between. Interestingly, if SRakes are used, 10 paths of Or_SRake and 20 paths of Op_SRake can capture most of the energy captured by Or_ARake and Op_ARake respectively in all three CMs. However, the energy capture becomes saturated gradually in all cases as L_c becomes large.

B. Performance vs. Complexity

Figure 14 shows the BEP performance of SRake receivers (L_c = 4 & 8) for BPSK. According to the results in Fig. 13, the Or_SRake results experience saturation earlier than Op_SRake and the rate of increment of energy capture is the fastest while L_c is below 10 in both cases. So, to be able to make comparison, we present the results of Fig. 14 for L_c = 4 and 8. It is seen from the results of CM1 in

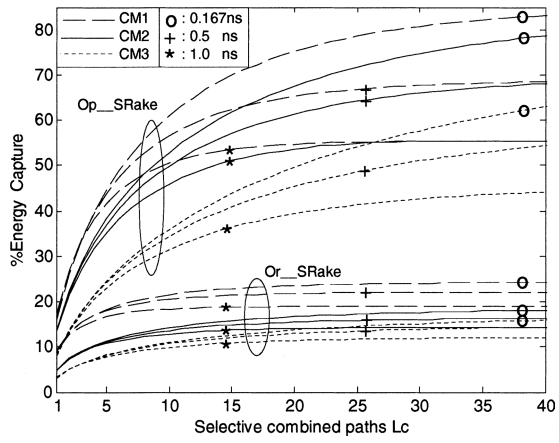

Fig. 13 Percent energy capture vs. number of selective combined paths L_c over CM1, CM2 and CM3. SNR = 20 dB and the modulation is BPSK.

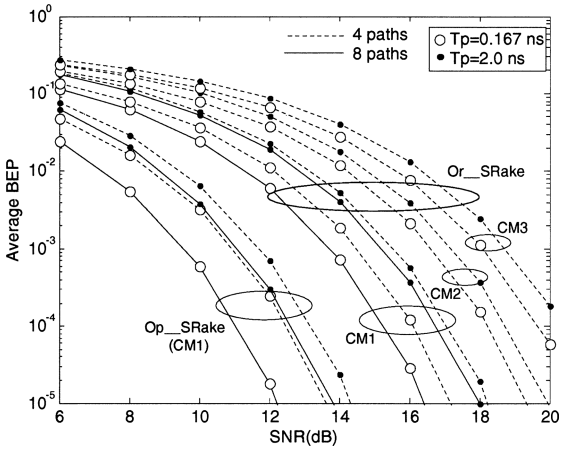

Fig. 14 BEP of Op_SRake (L_c = 4 and 8) and Or_SRake (L_c = 4 and 8) in CM1, and Or_SRake (L_c = 4) in CM2 and 3. The modulation is BPSK.

Fig. 14 that if the locations of the best paths can be estimated optimally, Op_SRake can provide considerable performance improvement as compared to Or_SRake with same L_c. Additionally, Op_SRake gains more performance improvement for increasing L_c from 4 to 8. Moreover, Op_SRake with L_c = 4 offers better performance than Or_ARake. For example, from Fig. 7, the required SNR at BEP = 10^{-5} is 18 dB for Or_ARake in the case of T_p = 2.0 ns. In contrast, from Fig. 14, the required SNR at the same BEP is 14.3 dB for Op_SRake (L_c = 4), which is 3.7 dB lower even though the number of combined paths is much smaller than Or_ARake.

Let's now take a different look on the matter. Op_SRake results as presented in Fig. 14, experience considerable performance degradation as compared with Op_ARake performances presented in Fig. 7. But, Or_SRake experiences much less degradation in a similar comparison with Or_ARake. If Rake complexity is simplified, increased SNR would be necessary to maintain the same BEP performance. This gives us a way to find out the cost incurred in SNR (dB) for simplifying Rake complexity at any specific BEP. Some of the results are listed in Table 4.

Table 4 Cost incurred in SNR to simplify Rake complexity. (CM1, BPSK and BEP = 10^{-5})

Complicated one	to	Simpler one	Cost in SNR (dB)		
			T_p = 167 ps	T_p = 1 ns	T_p = 2 ns
Op_ARake	→	*Or_ARake*	−5.15	−4.29	−4.15
*Op_SRake*8	→	*Or_SRake*8	−4.20	−4.13	−4.26
*Op_SRake*4	→	*Or_SRake*4	−3.56	−3.62	−3.92
Op_ARake	→	*Op_SRake*8	−1.32	−0.20	0.00
	→	*Op_SRake*4	−2.74	−1.24	−0.47
Or_ARake	→	*Or_SRake*8	−0.37	−0.04	0.00
	→	*Or_SRake*4	−1.15	−0.57	−0.24

Table 5 Cost incurred in SNR (dB) to simplify Or_ARake by Or_SRake. (L_c = 4) (BPSK and BEP = 10^{-5})

	T_p = 0.167 ns	T_p = 2.0 ns
CM1	−1.15 (dB)	−0.24 (dB)
CM2	−2.35 (dB)	−0.90 (dB)
CM3	−3.80 (dB)	−1.80 (dB)

The cost depends on the pulse-width T_p. When an ARake is simplified by another ARake of the simpler kind, or by an SRake of the same kind, the cost decreases for using wider T_p. However, when an Op_SRake is simplified by an Or_SRake (having the same number of combined paths L_c), there seems to be an optimum T_p for which the cost is minimum. A close inspection on a more detail set of data reveals that the optimum value of T_p is around 1.0 ns for L_c = 8 and below 0.167 ns for L_c = 4. Additionally, the cost in SNR for simplifying an ARake by an SRake depends on the channel model. Table 5 shows some results for an Or_ARake being simplified by an Or_SRake (L_c = 4). As the channel model changes from CM1 to CM2 and to CM3, the cost increases because the total energy becomes scattered over more number of paths and the power delay profiles (PDP) of the channels go a bit flatter [18], [26].

Finally, there is another interesting finding from Table 4 that the cost of simplifying an Op_SRake (L_c = 4) by an Or_SRake (L_c = 4) is less than that in simplifying an Op_ARake by an Or_ARake. Note also from Fig. 14 that Or_SRake (L_c = 4) performs quite well over all channel models as long as reasonably high SNR can be maintained. This would draw attention to Or_SRake (L_c = 4) because of its implementation simplicity.

C. Or_SRake Performance vs. Pulse-Width

In Fig. 15 we present BEP vs. pulse-width for communications using Or_SRake (L_c = 4) over CM1 to 3. SNR is set at 20 dB and BPSK is used. Best BEP performances are obtained at pulse-widths (i.e. the optimum pulse-widths) around 0.2 ns for CM1, 0.3 ns for CM2 and 0.5 ns for CM3. This can be more clearly seen from Fig. 16 that shows a magnified version of Fig. 15. For an SRake with certain L_c, wider pulses are supposed to supply more fractional energy, but they experience more fading. Oppositely, shorter pulses though possess less energy experience less fading. This trade-off is supposed to provide an optimum pulse-width for UWB communications using SRake [17], [26]–[28]. The optimum pulse-width is defined as the pulse-width using which provides the minimum achievable BEP performance at any specified SNR. However, here for L_c = 4, when the pulse-width becomes shorter than 1.0 ns, the performance variation is very small, especially in CM2 and 3 (see Fig. 15).

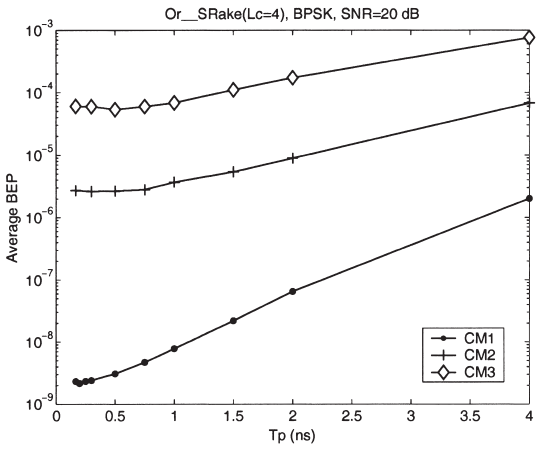

Fig. 15 BEP vs. pulse-width for Or_SRake (L_c = 4) in CM1, 2 and 3. The modulation in BPSK and SNR = 20 dB.

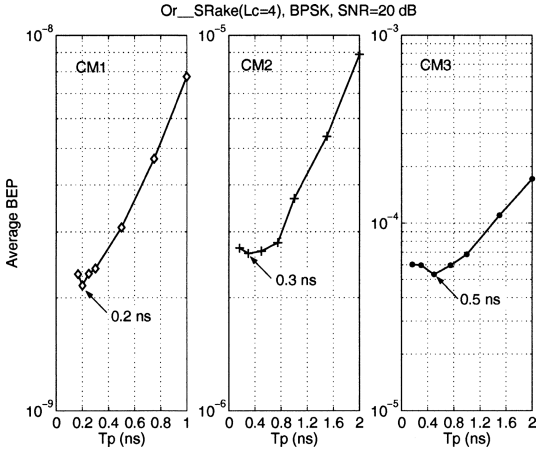

Fig. 16 BEP vs. pulse-width for Or_SRake (L_c = 4) in CM1, 2 and 3. The modulation in BPSK and SNR = 20 dB. Magnified version of Fig. 15.

Finally, it should be noted that the optimum pulse-widths presented in this paper are solely based on IEEE 802.15.3a channel models and pulse shape as shown in Fig. 3. Use of different pulse shapes and different channel models will lead to different optimum pulse-widths. Note also that optimum pulse-width also depends on L_c, operating SNR, the channel characteristics i.e. maximum delay spread, PDP etc. [26], [27] and antenna characteristics that may modify the pulse shape.

D. The Guarantee of Performance

For practical purposes, especially for commercial applications, a high guarantee of performance may be desired. Figure 17 presents the cumulative distribution function (cdf) curves for BEP of Or_SRake (L_c = 4) in CM1, 2 and 3. SNR

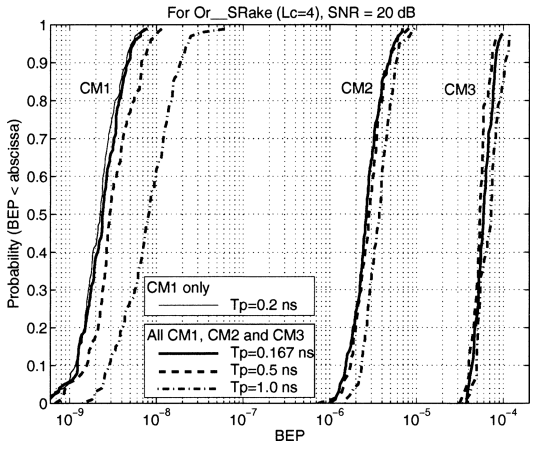

Fig. 17 Cumulative distribution curves of BEP for Or_SRake ($L_c = 4$) in CM1, 2 and 3. The modulation in BPSK and SNR = 20 dB.

is set at 20 dB and BPSK is used. Figure 17 can be used to obtain the BEP at any specific desired guarantee level. For example, Fig. 16 shows the average BEP of Or_SRake ($L_c = 4$) to be around 2.15×10^{-9} for $T_p = 0.2$ ns (which is the optimum value) in CM1. However from Fig. 17, we may take a further decision that in CM1, at 20 dB SNR, BEP of 4.45×10^{-9} or less is guaranteed with a probability of 90% for the same pulse-width.

5. Conclusions

Performance of ordinary and optimum Rake receiver have been investigated in TH-MPPM and TH-BPSK UWB communications. The SEP have been derived and those results have been used to simulate the performance of Rake reception of UWB signals over realistic multipath channels. The performances of various Rake receivers were compared for several modulation schemes and pulse-width over various channel models. The pulse-width has been identified as an important system parameter that, in general, affects Rake performance. Optimum Rakes have been shown to perform better than the ordinary counterpart, because the estimation of path delay brings more fractional energy capture. It has been shown that if the path delay estimation is available in spite of increasing system complexity, Op_SRake with only 4 paths offers better performance than Or_ARake. However, from performance vs. complexity trade-off point of view, Or_SRake may appear to be attractive.

Acknowledgments

This work was supported in part by the Grant-in-Aid for scientific research (No. 16560328) of JSPS, International Communication Foundation (ICF) and Union Tool Scholarship Foundation of Japan. Graduate studies of Mr. Rahman are funded by the Government of Japan under the Monbukagakusho scholarship program.

References

[1] D. Porcino and W. Hirt, "Ultra-wideband radio technology: Potential and challenges ahead," IEEE Commun. Mag., vol.41, no.7, pp.66–74, July 2003.
[2] R.A. Scholtz, "Multiple access with time-hopping impulse modulation," Proc. MILCOM, vol.2, pp.447–450, Boston, MA, Oct. 1993.
[3] M.Z. Win and R.A. Scholtz, "Characterization of ultra-wide bandwidth wireless indoor channels: A communication-theoretic view," IEEE J. Sel. Areas Commun., vol.20, no.9, pp.1613–1627, Dec. 2002.
[4] J.G. Proakis, Digital Communications, 4th ed., McGraw Hill, New York, 2001.
[5] M.Z. Win and R.A. Scholtz, "On the energy capture of ultrawide bandwidth signals in dense multipath environments," IEEE Commun. Lett., vol.2, no.9, pp.245–247, Sept. 1998.
[6] M.Z. Win and Z.A. Kostic, "Impact of spreading bandwidth on Rake reception in dense multipath channels," IEEE J. Sel. Areas Commun., vol.17, no.10, pp.1794–1806, Oct. 1999.
[7] M.Z. Win, G. Chrisikos, and N.R. Sollenberger, "Performance of Rake reception in dense multipath channels: Implications of spreading bandwidth and selection diversity order," IEEE J. Sel. Areas Commun., vol.18, no.8, pp.1516–1525, Aug. 2000.
[8] F. Ramirez-Mireles, M.Z. Win, and R.A. Scholtz, "Signal selection for the indoor wireless impulse radio channel," Proc. 47th VTC 1997, vol.3, pp.2243–2247, May 1997.
[9] J.D. Choi and W.E. Stark, "Performance of ultra-wideband communications with suboptimal receivers in multipath channels," IEEE J. Sel. Areas Commun., vol.20, no.9, pp.1754–1766, Dec. 2002.
[10] D. Cassioli, M.Z. Win, F. Vatalaro, and A.F. Molisch, "Performance of low-complexity Rake reception in a realistic UWB channel," Proc. ICC 2002, vol.2, pp.763–767, April/May 2002.
[11] A. Rajeswaran, V.S. Somayazulu, and J.R. Foerster, "Rake performance for a pulse based UWB system in a realistic UWB indoor channel," Proc. ICC 2003, vol.4, pp.2879–2883, 2003.
[12] B. Mielczarek, M.O. Wessman, and A. Svensson, "Performance of coherent UWB Rake receivers using different channel estimators," Proc. IWUWBS 2003, CD ROM, June 2003.
[13] J. Zhang, R.A. Kennedy, and T.D. Abhayapala, "Performance of Rake reception of ultra wideband signals in a lognormal-fading channel," Proc. IWUWBS 2003, CD ROM, June 2003.
[14] H. Sheng, A.H. Haimovich, A.F. Molisch, and J, Zhang, "Optimum combining for time hopping impulse radio UWB Rake receivers," Proc. UWBST 2003, pp.224–228, Nov. 2003.
[15] F. Ramirez-Mireles, M.Z. Win, and R.A. Scholtz, "Performance of ultra-wideband time-shift-modulated signals in the indoor wireless impulse radio channel," Proc. 1998 Asilomar Conf., pp.192–196, 1998.
[16] S. de Rivaz, B. Denis, J. Keignart, M. Pezzin, N. Daniele, and D. Morche, "Performances analysis of a UWB receiver using complex processing," Proc. UWBST 2003, pp.229–233, Nov. 2003.
[17] M.A. Rahman, S. Sasaki, J. Zhou, S. Muramatsu, and H. Kikuchi, "Performance evaluation of Rake reception of ultra wideband signals over multipath channels from energy capture perspective," Proc. Joint UWBST and IWUWBS 2004, pp.231–235, May 2004.
[18] J. Foerster, "Channel modeling sub-committee report final," IEEE P802.15-02/368r5-SG3a, Dec. 2002.
[19] J.M. Wozencraft and I.M. Jacobs, Principles of Communication Engineering, John Wiley, 1965.
[20] L. Ge, G. Yue, and S. Affes, "On the BER performance of pulse-position-modulation UWB radio in multipath channels," Proc. UWBST 2002, pp.231–234, May 2002.
[21] A.A.M. Saleh and A. Valenzuela, "A statistical model for indoor multipath propagation," IEEE J. Sel. Areas Commun., vol.SAC-5, no.2, pp.128–137, Feb. 1987.
[22] J. Foerster and Q. Li, "UWB channel contribution from Intel," IEEE

P802.15-02/279r0-SG3a, March 2003.

[23] R.C. Larson and A.R. Odoni, Urban Operations Research, chapter 2, Prentice-Hall, New Jersey, 1981, available at http://web.mit.edu/urban_or_ book/www/book.

[24] A.F. Molisch, J.R. Foerster, and M. Pedergrass, "Channel models for ultrawideband personal area networks," IEEE Wirel. Commun., vol.10, no.6, pp.14–21, Dec. 2003.

[25] T.S. Rappaport, Wireless Communications: Principles and Practice, section 4.2.1., Prentice Hall, New Jersey, 1996.

[26] M.A. Rahman, S. Sasaki, J. Zhou, S. Muramatsu, and H. Kikuchi, "Evaluation of selective Rake receiver in direct sequence ultra wideband communications," IEICE Trans. Fundamentals, vol.E87-A, no.7, pp.1742–1746, July 2004.

[27] W.C. Lau, M.S. Alouini, and M.K. Simon, "Optimum spreading bandwidth for selective Rake reception over Rayleigh fading channels," IEEE J. Sel. Areas Commun., vol.19, no.6, pp.1080–1089, June 2001.

[28] D. Cassioli, M.Z. Win, and A.F. Molisch, "Effects of spreading bandwidth on the performance of UWB Rake receivers," Proc. ICC 2003, vol.5, pp.3545–3549, 2003.

Mohammad Azizur Rahman received his Bachelor's degree in Electrical and Electronic Engineering (EEE) in August 2001 from Bangladesh University of Engineering and Technology (BUET), Dhaka, Bangladesh. From August 2001 to March 2002 he served as a Lecturer in the Department of EEE of the same university. From April 2002, he is attached with Niigata University, Niigata, Japan as a Japanses Government (Monbukagakusho) scholar. In October 2002, he entered the Department of EEE of the university as a research student, where he later in April 2003 entered as a Master's degree student. He is presently working toward a Doctoral degree in the same place. His research interests include Spread Spectrum and Ultra Wideband Communications, Communication Theory, Rake and Diversity Receivers, Signaling Design, Multiple Access Communications etc. Mr. Rahman is a student member of the IEEE.

Shigenobu Sasaki received B.E., M.E. and Ph.D. degrees from Nagaoka University of Technology, Nagaoka, Japan, in 1987, 1989 and 1993, respectively. Since 1992, he has been with Niigata University, where he is now an Associate Professor in the Department of Electrical and Electronic Engineering. From 1999 to 2000, he was a visiting scholar at the Department of Electrical and Computer Engineering, University of California, San Diego. Since 2003, he has been with the UWB technology institute, National Institute of Information and Communication Technology (NICT) as an expert researcher. His research interests are in the area of digital communications with special emphasis on spread spectrum communication systems, ultra-wideband communication systems and wireless communications. He is a member of the IEEE and SITA.

Jie Zhou was born in Sichuan, China, in 1964. He received B.E and M.E degrees from Nanjing University of Posts and Telecommunications, China in 1985 and 1990, respectively and Dr. Eng. degree from the Department of Computer Science, Gunma University, Japan in March 2001. Afterwards, he joined Chongqing University of Posts and Telecommunications, where he became an engineer in 1992 and an associate professor in 1998. From April 2001 to March 2005, he was with the Department of Electrical and Electronic Engineering, Niigata University, Japan where he was a Research Associate. Since March 2005, he has been with the Department of Information and Communications, Nanjing University of Information Science and Technology, where he is currently a Professor. His research interests lie in the areas of DATA, ATM and radiowave propagation in mobile communications.

Hisakazu Kikuchi received the B.E. and M.E. degrees from Niigata University in 1974 and 1976, respectively, and Dr. Eng. degree in electrical and electronic engineering from Tokyo Institute of Technology in 1988. From 1976 to 1979 he worked at Information Processing Systems Laboratory, Fujitsu Ltd., Tokyo. Since 1979 he has been with Niigata University, where he is a professor of electrical engineering. He was a visiting professor at Electrical Engineering Department, University of California, Los Angeles during a year of 1992 to 1993. He holds a visiting professorship at Chongqing University of Posts and Telecommunications, China since 2002. His research interests are in digital signal processing and image/video processing as well as ultra wideband systems. Dr. Kikuchi is a member of the ITEJ (Institute of Image Information and Television Engineers of Japan), IIEEJ (Institute of Image Electronics Engineers of Japan), JSIAM (Japan Society for Industrial and Applied Mathematics), RISP (Research Institute of Signal Processing), IEEE, and SPIE. He served the chair of Circuits and Systems Group, IEICE, in 2000 and the general chair of Digital Signal Processing Symposium, IEICE, in 1988 and Karuizawa Workshop on Circuits and Systems, IEICE, in 1996.